unaffected, even though the film has a capacity for considerable further charging. Whatever the chemical nature of the changes that occur at potentials more positive than +0.1 to 0.2 V, they apparently do not significantly alter the structural features of poly(pyrrole) that determine its electrical conductivity.

The potential dependency of the *ionic* conductivity of poly(pyrrole) seems to parallel the electrical conductivity. That is, the most striking changes in ionic conductivity[18] also occur at potentials more negative than about 0 V, and so the chemical events that lead to major changes in ionic and electrical conductivity appear to be related. In the simplest of interpretations, a reduced poly(pyrrole) chain (or ensemble thereof) becomes electrically conducting by becoming oxidized and cationic; the latter property in turn produces a permeability of the polymer structure to anionic counterions.

Finally, the nonlinear relationship between poly(pyrrole) conductivity and charge (oxidation state) expressed in Figures 2 and 9 suggests that poly(pyrrole) electrical conductivity may be determined by different limiting factors depending on the film oxidation state. The various conductivity controlling factors which have been suggested include the population of bipolarons,[25,34] the percentage of chains or segments thereof which are oxidized (chain oxidation state being a function of chain length at a given potential),[35] and the rate of electron hopping between chains or across chain defects.[36] The result of Figure 9 thus suggests a possible shift of control between two of the above (or some other) factors.

Acknowledgment. This research was supported in part by grants from the National Science Foundation and the Office of Naval Research.

(34) Bredas, J. L.; Themans, B.; and Andre, J. M., *Phys. Rev. B.*, **1983**, *27*, 7827.
(35) Bredas, J. L.; Silbey, R.; Boudreaux, D. S.; and Chance, R. R., *J. Am. Chem. Soc.* **1983**, *105*, 6555.
(36) Tanaka, M.; Watanabe, A.; Fujimoto, H.; and Tanaka, J. *Mol. Cryst. Liq. Cryst.*, **1982**, *83*, 277.

Charge Density Topological Approach to the Dinorcaradiene $\rightleftharpoons$ [10]Annulene Equilibrium in Some 11,11-Disubstituted 1,6-Methane[10]annulenes

Carlo Gatti, Mario Barzaghi, and Massimo Simonetta*

Contribution from the C.N.R. Center for the Study of Structure/Reactivity Relations and Department of Physical Chemistry and Electrochemistry, University of Milan, 20133 Milan, Italy. *Received August 7, 1984*

Abstract: The topological theory of molecular structure is used to analyze the electronic charge distribution in some 11-R-11-R′-1,6-methane[10]annulenes (R = R′ = H, CH_3, CN, F; R = CH_3, R′ = CN). The presence of the C_1–C_6 bond critical point in the dicyano derivative and in the β phase of the methylcyano derivative points out the dinorcaradienic character of these compounds. Of the two different molecules in the crystal unit cell of the dimethyl derivative, one has a dinorcaradienic structure (but with a very low C_1–C_6 bond order, $n = 0.44$) and the latter has an annulenic structure (since the C_1–C_6 bond critical point has disappeared). These facts indicate the existence of a bifurcation catastrophe point as well as a maximum in the free molecular potential, in the range of experimental geometries, along the reaction coordinate of the valence tautomerism between the dinorcaradienic and the annulenic structures. Comparison with the topological results of the related 1,1-disubstituted cyclopropanes allows an exhaustive description of the conjugative coupling of the cyclopropyl ring with the two butadienyl fragments linked to it. When the C_1–C_6 bond length is close to the value of normal CC bonds, the π-like charge distribution of the three-membered ring system is preserved and the whole cyclopropyl ring behaves as a conjugate π bond. However, as the C_1–C_6 bond lengthens, the three-membered ring critical point approaches the critical point of the C_1–C_6 bond, thereby reducing its bond order and enhancing its ellipticity (i.e., its π character). This mechanism, at its extreme consequences, leads to the annulenic structure. In the annulenic derivatives, beside the fundamental 10π-electron aromatic system, a conjugative coupling of the cyclopropyl ring to the [10]annulenic framework, involving the two external bonds of the three-membered ring, is still of some relevance.

In the last years the geometry of a number of 1,6-methane[10]annulene derivatives has been determined in our X-ray laboratory[1-7] in connection with the study of the equilibrium [10]annulene $\rightleftharpoons$ dinorcaradiene (1). The variation of the C_1–C_6 bond length, as a function of the substituents at C_{11}, is the most relevant geometrical aspect of a less evident but systematic variation of all the structural parameters. A qualitative explanation[3-6] of the

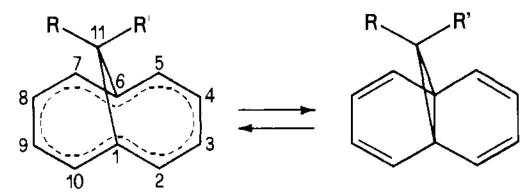

(1)

observed trend in the bridgehead carbon atoms distance was afforded by comparison with the corresponding C_2–C_3 distance variations in a series of 1,1-disubstituted cyclopropanes. In fact it is well-known[8a,b] that the introduction of π-donating groups at carbon C_1 in the cyclopropane ring lengthens all the CC bonds in the ring, while π-acceptor substituents shorten the C_2–C_3 bond and lengthen the other two. A qualitative description of these

(1) Bianchi, R.; Pilati, T.; Simonetta, M. *Acta Crystallogr., Sect.B* **1980**, *B36*, 3146.
(2) Pilati, T.; Simonetta, M. *Acta Crystallogr., Sect. B* **1976**, *B32*, 1912.
(3) Bianchi, R.; Pilati, T.; Simonetta, M. *Acta Crystallogr., Sect. C* **1983**, *C39*, 378.
(4) Bianchi, R.; Morosi, G.; Mugnoli, A.; Simonetta, M. *Acta Crystallogr., Sect. B* **1973**, *B29*, 1196.
(5) Bianchi, R.; Pilati, T.; Simonetta, M. *Acta Crystallogr., Sect. B* **1978**, *B34*, 2157.
(6) Bianchi, R.; Pilati, T.; Simonetta, M. *J. Am. Chem. Soc.* **1981**, *103*, 6426.
(7) Bianchi, R.; Spackman, M. A.; Stewart, R. F. *J. Am. Chem. Soc.*, submitted.

(8) (a) Hoffman, R. *Proc. Int. Congr. Pure Appl. Chem.* **1971**, *23*, 233. (b) Hoffman, R.; Davidson, R. B. *J. Am. Chem. Soc.* **1971**, *93*, 5699. (c) Hoffman, R. *Tetrahedron Lett.* **1970**, 2907.

Table I. List of the Investigated Structures

shorthand notation	molecular structure	$R_{C_1-C_6}$,[a] Å	ref
DIC	11,11-dicyanotricyclo[4.4.1.0^{1,6}]undeca-2,4,7,9-tetraene, at −123 °C	1.543	3
β-MC(1636)	11-methyltricyclo[4.4.1.0^{1,6}]undeca-2,4,7,9-tetraene-11-carbonitrile, β phase at −100 °C	1.636	6
β-MC(1712)	11-methyltricyclo[4.4.1.0^{1,6}]undeca-2,4,7,9-tetraene-11-carbonitrile, β phase	1.712	6
DIM(1770)[b]	11,11-dimethyltricyclo[4.4.1.0^{1,6}]undeca-2,4,7,9-tetraene	1.770	4
α-MC(1783)[b]	11-methyltricyclo[4.4.1.0^{1,6}]undeca-2,4,7,9-tetraene-11-carbonitrile, α phase	1.783	5
DIM(1826)[b]	11,11-dimethyltricyclo[4.4.1.0^{1,6}]undeca-2,4,7,9-tetraene	1.826	4
α-MC(1850)[b]	11-methyltricyclo[4.4.1.0^{1,6}]undeca-2,4,7,9-tetraene-11-carbonitrile, α phase	1.850	5
MET	1,6-methane[10]annulene, at −128 °C	2.235	1
DIF	11,11-difluoro-1,6-methane[10]annulene, at −100 °C	2.269	2

[a] If not otherwise stated, all data refer to room temperature. [b] Compounds with two different molecules in the crystal unit cell.

effects was firstly provided by Hoffman[8c] in terms of the interaction of the HOMO and LUMO of the substituent at C_1 with the Walsh orbitals[9] of cyclopropane.

More recently, such an interpretation was generalized to include more specific effects of the substituent (as in the case of fluorine).[10a] In particular, the relevance of both the σ- and π-acceptor/donor properties of the substituent in the interaction with the Walsh orbitals was pointed out.[11] In addition, the interaction between the substituents and the cyclopropyl ring through orbitals of proper symmetry which are lower in energy than the Walsh orbitals was also found to be of importance.[10]

Very recently, Bader has shown[12-16] that the properties of the molecular charge density at its critical points provide an unambigous description of the molecular structure and its susceptibility to possible structural changes. Such a description, in spite of some apparent complexity of its mathematical formulation, has the main advantage to introduce in a quite rigorous and quantitative way concepts and quantities which are very close to the usual feeling of the chemists. It allows the predicted electronic effects to be translated into observable consequencies in the charge distribution.

The variations of the charge density associated with the opening of a ring structure by lengthening of a ring bond has been investigated by Bader and co-workers through a topological analysis of the molecular charge distribution of cyclopropane (a three carbon membered ring, 3MR).[12] Bader's results provide a physical basis to the π functionality of the cyclopropane ring in terms of substantial in-plane bond ellipticities and give an insight into the possible ways in which a 3MR can be conjugatively linked to an unsaturated system. Progressive lengthening of a CC bond of cyclopropane from its equilibrium distance involves a transition, in the space of nuclear configurations, between different *structural regions*,[13] which are both characterized by a unique set of critical points. Any transition between two regions whose structure is stable from a topological point of view implies that the molecular system goes through a catastrophe configuration.[13,17] A similar situation is expected for the valence tautomerism of eq 1. The substituents at the bridging carbon atom can be regarded as a set of discrete control parameters which define specific positions of the 1,6-methane[10]annulene skeleton inside the two regions of structural stability. So, in a topological sense the substituent effect may sketch the reaction coordinate for the transition from the dinorcaradienic structure to the [10]annulenic one.

In this paper we present a description of the topological properties of the electron density of some derivatives of 1,6-methane[10]annulene (see Table I) evaluated by the ab initio single-determinant SCF method. In particular, the aim of this work is to describe (i) the geometrical changes, the strains, and the deformation of the charge distribution induced in a cyclopropyl ring after its insertion in the [10]annulenic skeleton, (ii) the progressive variation of the overall properties of the charge density, in connection with the systematic geometrical changes, which are observed on going from the dinorcaradienic to the annulenic structure through the effect of different substituents, and (iii) the susceptibility of the charge distribution to experience structural changes. With regard to the last point, it is noteworthy that those compounds which have more than one stable phase[5,6] and/or two different molecules in their crystal unit cell[4,5] have geometrical arrangements which closely correspond to a catastrophe configuration.

The conjugative coupling of the cyclopropyl ring with unsaturated fragments can be considered on the basis of three limiting interactions; namely (i) the whole cyclopropyl ring takes the place of a double bond to realize a delocalization of charge through conjugation (in this case the perturbation of the ring charge density is relatively slight and the surface of delocalization in the 3MR is preserved), (ii) the C_1–C_6 bond conjugatively participates to the two 6MR's and (iii) only the two external bonds of the cyclopropyl ring are coupled conjugatively with the unsaturated fragment. These three possibilities occur in vinylcyclopropane,[12] in the homotropylium cation,[14] and in the bicyclo[3.1.0]hexenyl cation,[14] respectively. In our systems the different substituents at C_{11} dictate the conjugative mechanism of the cyclopropyl ring with the two butadienyl fragments linked to the carbon atoms 1 and 6.

The quantities and concepts of the topological theory of molecular structure which are of relevance to the following discussion will be briefly summarized in the Appendix section.

Methods

Ab initio calculations were performed with the GAUSSIAN 80 system of programs,[18] using a minimal (STO-3G)[19] or a split valence (3-21G)[20] basis set. The geometries of 1,1-disubstituted cyclopropanes and norcaradiene were fully optimized (at both the STO-3G and 3-21G levels) by means of analytically evaluated gradients.[21] The 11,11-disubstituted 1,6-methane[10]annulenes were calculated at the STO-3G level by using the experimental X-ray geometries.[1-6] The symmetric and the asymmetric disubstituted derivatives were constrained to C_{2v} and C_s symmetry, respectively. All the CH bond distances were fixed at 1.08 Å. A shorthand notation (hereafter adopted) for the investigated compounds is reported in Table I. For some systems more than one geometry was considered, as the experimental data refer to different crystal phases (MC molecule)[5,6] or to the two geome-

(9) (a) Walsh, A. D. *Nature (London)* **1947**, *159*, 167, 712. (b) Walsh, A. D. *Trans. Faraday Soc.* **1949**, *45*, 179.

(10) (a) Skancke, A.; Boggs, J. E. *J. Mol. Struct.* **1977**, *40*, 263. (b) Skancke, A. *J. Mol. Struct.* **1977**, *42*, 235.

(11) Durmaz, S.; Kollmar, H. *J. Am. Chem. Soc.* **1980**, *102*, 6942.

(12) Bader, R. F. W.; Slee, T. S.; Cremer, D.; Kraka, E. *J. Am. Chem. Soc.* **1983**, *105*, 5061.

(13) Bader, R. F.; Nguyen-Dang, T. T.; Tal, Y. *Rep. Progr. Phys.* **1981**, *44*, 893.

(14) Cremer, D.; Kraka, E.; Slee, T. S.; Bader, R. F. W.; Lau, C. D. H.; Nguyen-Dang, T. T.; MacDougall, P. J. *J. Am. Chem. Soc.* **1983**, *105*, 5069.

(15) Bader, R. F. W.; Tang, T.; Tal, Y.; Biegler-König, F. W. *J. Am. Chem. Soc.* **1982**, *104*, 946.

(16) Bader, R. F. W.; Tang, T.; Tal, Y.; Biegler-König, F. W. *J. Am. Chem. Soc.* **1982**, *104*, 940.

(17) Bader, R. F. W.; Nguyen-Dang, T. T.; Tal, Y. *J. Chem. Phys.* **1979**, *70*, 4316.

(18) A slightly modified version of the GAUSSIAN 80 series of programs for Gould S.E.L. computers was used. Binkley, J. S.; Whiteside, R. A.; Krishnan, R.; Seeger, R.; DeFrees, D. J.; Schlegel, H. B.; Topiol, S.; Kahn, L. R.; Pople, J. A. *QCPE* **1981**, *13*, 406.

(19) (a) Hehre, W. J.; Stewart, R. F.; Pople, J. A. *J. Chem. Phys.* **1969**, *51*, 2657. (b) Hehre, W. J.; Ditchfield, R.; Stewart, R. F.; Pople, J. A. *Ibid.* **1970**, *52*, 2769.

(20) (a) Binkley, J. S.; Pople, J. A.; Hehre, W. J. *J. Am. Chem. Soc.* **1980**, *102*, 939. (b) Gordon, M. S.; Binkley, J. S.; Pople, J. A.; Pietro, W. J.; Hehre, W. J. *Ibid.* **1982**, *104*, 2797.

(21) Schlegel, H. B. *J. Comput. Chem.* **1982**, *3*, 214.

Table II. CC Bond and Ring Critical Point Data for Some 1,1-Disubstituted Cyclopropanes Evaluated with STO-3G (3-21G) Fully Optimized Geometries

1,1-substituents			R_e, Å						
R	R′	critical point	calcd	exptl	$\rho(\mathbf{r}_c)$, au^{-3}	$\nabla^2\rho(\mathbf{r}_c)$, au^{-5}	λ_3, au^{-5}	$\epsilon = \lambda_1/\lambda_2 - 1$	n
H	H		1.502 (1.513)	1.510,[a] 1.514[b]	0.241 (0.218)	−0.613 (−0.477)	0.159 (0.210)	0.112 (0.171)	1.00
CN	CN		1.526 (1.537)		0.228 (0.208)	−0.516 (−0.399)	0.183 (0.222)	0.157 (0.226)	0.89
CH_3	CH_3[c]	C_1–C_2	1.508 (1.510)		0.240 (0.224)	−0.600 (−0.505)	0.170 (0.204)	0.113 (0.152)	0.99
CH_3	CN[c]		1.516 (1.521)		0.235 (0.218)	−0.571 (−0.470)	0.173 (0.208)	0.132 (0.186)	0.95
F	F		1.511 (1.469)	1.464[d]	0.239 (0.249)	−0.580 (−0.618)	0.195 (0.253)	0.112 (0.122)	0.98
CN	CN		1.495 (1.493)	1.485[e]	0.246 (0.229)	−0.640 (−0.543)	0.156 (0.206)	0.059 (0.094)	1.04
CH_3	CH_3[c]		1.504 (1.521)		0.241 (0.213)	−0.610 (−0.445)	0.160 (0.210)	0.115 (0.201)	1.00
CH_3	CN[c]	C_2–C_3	1.500 (1.508)		0.243 (0.221)	−0.625 (−0.491)	0.158 (0.208)	0.088 (0.148)	1.02
F	F		1.518 (1.549)	1.553[d]	0.236 (0.200)	−0.580 (−0.368)	0.169 (0.228)	0.084 (0.221)	0.95
H	H				0.182 (0.164)	0.208 (0.261)	0.243 (0.271)		
CN	CN				0.177 (0.164)	0.210 (0.252)	0.272 (0.302)		
CH_3	CH_3[c]	3MR			0.180 (0.166)	0.215 (0.260)	0.251 (0.282)		
CH_3	CN[c]				0.179 (0.166)	0.213 (0.255)	0.256 (0.280)		
F	F				0.176 (0.168)	0.249 (0.296)	0.269 (0.315)		

[a] Bastiansen, O.; Fritsch, F. N.; Hedberg, K. *Acta Crystallogr.* **1964**, *17*, 538. [b] Jones, W. J.; Stoicheff, B. P. *Can. J. Phys.* **1964**, *42*, 2259. [c] Methyl hydrogens are in a staggered arrangement with respect to the adjacent carbon, acording to experiment.[4-6] [d] Reference 25. [e] Pearson, R., Jr.; Choplin, A.; Laurie, V.; Schwartz, J. *J. Chem. Phys.* **1975**, *62*, 2949.

trically distinct molecules present in the same unit cell (DIM[4] and α-MC[5]).

The topological theory of molecular structure[12-16] was used to analyze the charge density function by means of the AIMPAC package of programs.[22] The capability of the STO-3G minimal basis set calculations to reproduce the experimental geometries of hydrocarbons and in particular the observed trends in CC bond lengths, as well as in bond angles, is well established.[23,24] Therefore, experimental geometries, rather than fully optimized geometries, are not expected to modify significantly the quality of the results of the topological analysis of the charge density function (see next section).

1,1-Disubstituted Cyclopropanes. As the first step of the study of the effects of substituents in position 11 of 1,6-methane[10]-annulene, we have optimized the equilibrium geometries of some 1-R-1-R′-cyclopropanes (R = R′ = H, CN, CH_3, F; R = CH_3, R′ = CN), at both the STO-3G and 3-21G levels. The bond and ring critical point data for all the investigated cyclopropanes are listed in Table II, where the optimized CC bond lengths are also compared with the available experimental data. The split valence 3-21G basis set gives geometries which are in very nice agreement with the experimental data. The STO-3G optimized values are quite close to the 3-21G ones, with the only well-known exception of 1,1-difluorocyclopropane.[10a] In fact, while experiments and 3-21G results indicate a very short C_1–C_2 bond and a very long C_2–C_3 bond, the minimal basis set does not pratically differentiate the CC bonds and greatly underestimates the dipole moment (experimental 2.32,[25] 3-21G 2.59, STO-3G 1.39, all values in debye).[26]

As can be inferred by inspection of Table II, small bond length variations, with respect to cyclopropane, are obtained at the expense of more evident changes in the charge distribution. The values of $\rho(\mathbf{r}_b)$, $\nabla^2\rho(\mathbf{r}_b)$, and n (see the Appendix section for the definition of symbols) show that the C_2–C_3 bond in 1,1-dicyanocyclopropane is stronger, and furthermore it has a very low ellipticity value (ϵ = 0.06, about half the value of cyclopropane), which indicates an increase of its σ character with respect to cyclopropane. The C_1–C_2 and C_1–C_3 bonds lengthen and their π character increases (ϵ = 0.16), due to an induced conjugative interaction with the cyano groups, as indicated by the overlap of the major axes (see the Appendix section) of the C_1–C_2 and C_1–CN bonds, which amounts to 0.88. In addition, the surface of the 3MR, though maintaining its peculiar π-type charge distribution,[12] is slightly charge-depleted and more significantly polarized, as shown by the difference of the positive eigenvalues at the ring critical point, the most pronounced positive curvature being in the direction perpendicular to the stronger C_2–C_3 bond (λ_2/λ_3 = 0.77 vs. 1.00 in cyclopropane). This fact provides a further evidence of the increased σ character of the C_2–C_3 bond.

The charge distribution of 1,1-dimethylcyclopropane is not significantly different from that of cyclopropane, whereas the 1-methyl-1-cyano derivative exhibits the expected intermediate behavior between the dicyano derivative and cyclopropane. The asymmetric substitution at C_1 does not greatly polarize the charge distribution on the 3MR in a direction perpendicular to it: the ring critical point is less than 0.01 au far off the ring plane on the CN side of the molecule.

The preliminary calculations of this section yielded two main results. Firstly the bond length variations, and even more the peculiar topological features dictated by the substituents at C_1, appear to be a valuable tool to describe the properties of the cyclopropyl ring in the related 11,11-disubstituted 1,6-methane-[10]annulenes (see infra). Such properties may determine in turn the degree of dinorcaradienic character of the different systems. Secondly, comparison of the 3-21G and STO-3G optimized equilibrium geometries with the experimental ones confirm that the use of experimental geometries in a STO-3G study of the 11,11-disubstituted 1,6-methane[10]annulenes is a reliable assumption (with the mentioned exception of the fluorine derivative). A far better basis set, including polarization functions, should be demanded,[23,24,27] if one is interested in strain energy or in substituent stabilization energy estimation.

Effect of Substituents at C_{11}: Relevant Topological Variations of the Charge Density. In this section we analyze some relevant trends in the topological variations of the charge distribution of the investigated systems (Table I). We anticipate that these variations, which are simply dictated by the different substituents at C_{11}, are similar to those observed for the parent 1,6-methane[10]annulene along the (3-21G fully optimized) reaction

(22) Biegler-König, F. W.; Bader, R. F. W.; Tang, T. *J. Comput. Chem.* **1982**, *13*, 317.

(23) Pople, J. A. In "Modern Theoretical Chemistry"; Schaefer, H. F., III, Ed.; Plenum Press: New York, 1977; Vol. 3, pp 1–28.

(24) Newton, M. D. In "Modern Theoretical Chemistry"; Schaefer, H. F., III, Ed.; Plenum Press: New York, 1977; Vol. 4, pp 223–275.

(25) Perretta, A. T.; Laurie, V. W. *J. Chem. Phys.* **1975**, *62*, 2469.

(26) Throughout this paper only the STO-3G topological results for the disubstituted cyclopropanes will be discussed, as the disubstituted 1,6-methane[10]annulenes are evaluated with the same basis set. The agreement of the STO-3G and 3-21G basis sets in predicting the CC bond-length variations of 1-R-1-R′-cyclopropanes implies a similar agreement in the trend of the related topological features. A detailed analysis of the origin of the deficiencies of the STO-3G basis set for the fluorine derivatives is in progress both by means of conventional correlation diagrams, Walsh orbitals, and Mulliken population considerations and by means of a topological analysis of the whole charge density function as well as of the individual MO's.

(27) Hariharan, P. C.; Pople, J. A. *Chem. Phys. Lett.* **1972**, *16*, 217.

path for the valence tautomerism (1).[28,29] Therefore, such topological changes can be ascribed mainly to the transition from the dinorcaradienic to the [10]annulenic structure under the influence of the different substituents.

The CC bond and ring critical point data for all the investigated geometries are listed in Table III. The paths traced out by the gradient vector $\nabla\rho$ of the charge density ρ in the cyclopropyl plane are displayed in Figure 1.

The main interesting aspect of our results is the description of the C_1–C_6 bonding/nonbonding interaction. In this respect a first clear-cut indication stems from the existence of the C_1–C_6 bond critical point and the related cyclopropyl ring critical point in DIC, β-MC(1636), β-MC(1712), and DIM(1770).

On going from DIC to DIM(1770), the C_1–C_6 bond length increases, while the value of ρ at both the C_1–C_6 bond critical point and ring critical point decreases. Correspondingly the bond critical point moves from the external to the internal side of the C_1–C_6–C_{11} triangle and approaches the ring critical point, until they coalesce and finally disappear in α-MC(1783). This movement results from release of strain in the 3MR and from the progressive flattening of the charge density along the line joining the two critical points. Hence in α-MC(1783) the charge density doesn't exhibit a minimum anymore, and the line of maximum charge, which defines the C_1–C_6 bond path, has vanished accordingly, so that no residual bond links the atoms C_1 and C_6.

The lengthening of the C_1–C_6 bond until rupture is reflected in the dramatic decrease of the bond order n (cf. last column of Table III).[30] Also the ellipticity of the C_1–C_6 bond increases quickly as the bond lengthens, since the negative curvature (λ_2) of its major axis must vanish when the bond and ring critical points coalesce.[12] Therefore, the bond ellipticity can be regarded as a measure of the susceptibility of a CC ring bond to rupture.[12,14]

Another interesting feature of the topology of disubstituted 1,6-methane[10]annulenes is the position of the critical point of the six or seven carbon membered rings. These compounds can be envisaged as two 6MR's and one 3MR condensed on the C_1–C_6 bond (namely DIC, β-MC's, and DIM(1770)) or as two 7MR's which share the C_1–C_{11} and C_6–C_{11} bonds (α-MC's, DIM(1826), MET, and DIF). The extent of C_{11} participation to the 7MR can be quantified by the standard deviation, S, of the distances between the nuclei in each ring and the ring critical point. As shown in Table IV, S decreases from α-MC(1783) to DIF, as the ring carbon atoms become increasingly equivalent in nature. Accordingly the ring critical point moves out of the C_1–C_2–C_5 plane toward C_{11}, which in turn becomes more involved in the aromatic system.[31] Therefore, while in dinorcaradienic systems the 6MR surface is close to the plane of the corresponding nuclei, in the annulenic structures the ring surface of 7MR is strongly curved above the nuclei. This is indicated (cf. Table IV) by the clear-cut increase of the distance h between the ring critical point and the C_1–C_2–C_5 plane, from DIC (0.007 Å) to MET (0.314 Å). The motion of the ring critical point results from the progressive depletion of charge in the interior of the geometrical 6MR surface.

The asymmetric substitution at C_{11} in MC's differentiates markedly the charge distribution on the two rings, in spite of the close similarity of the equilibrium bond lengths. In fact, the charge is more attracted toward C_{11} and the cyclopropyl plane, in the ring below the cyano group (see h and l values in Table IV).

The charge density value at the 6MR critical point in DIC (0.0208 au^{-3}) is very close to the value of norcaradiene (0.0205 au^{-3}, STO-3G fully optimized geometry) and decreases systematically on going toward DIF (0.0137 au^{-3}). The charge decrease complies with the augmented flatness of the charge distribution on the ring surface and in the direction perpendicular to it, as can be argued from the curvature values (λ_i) at the ring critical point.

A quite distinctive mark of the aromatic character of the investigated systems is represented by the standard deviation, S_R, of the CC distances along the annulenic perimeter.[32] Table V shows that a parallel trend is exhibited by the standard deviation,

A

B

C

D

E

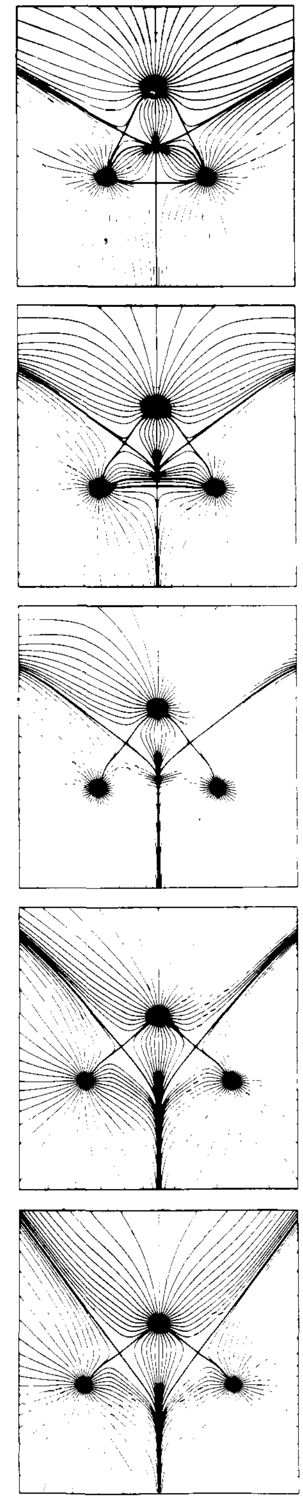

Figure 1. Phase portraits of the critical points in $\rho(\mathbf{r})$ for some 11,11-disubstituted 1,6-methane[10]annulenes in the plane of the cyclopropyl ring. The lines are the paths traced out by the gradient vector field $\nabla\rho(\mathbf{r})$. The bond paths and the trajectories which mark the intersections of the interatomic surfaces with the cyclopropyl plane are indicated by heavy lines: (A) DIC, (B) DIM(1770), (C) DIM(1826), (D) MET, and (E) DIF.

(28) Barzaghi, M.; Gatti, C.; Simonetta, M., unpublished results.

(29) Barzaghi, M.; Bianchi, R.; Gatti, C.; Simonetta, M. *Int. J. Quantum Chem. Symp.*, in press.

(30) n values were estimated through eq A3, which was obtained by fitting to more conventional CC bonds (n ranging from 1 to 3). Therefore, extrapolation to n values less than 1 should be considered with some care.

(31) In the case of the unsubstituted 1,6-methane[10]annulene, the 6/7MR critical point traverses the C_1–C_2–C_5 plane along the (3-21G fully optimized) reaction path from the dinorcaradienic to the annulenic structure.[28]

(32) Gavezzotti, A; Simonetta, M. *Helv. Chim. Acta*, **1976**, *59*, 2984.

Table III. CC Bond and Ring Critical Point Data for the 1,6-Methane[10]annulene Derivatives[a,b]

system	critical point	R_c, Å	$\rho(\mathbf{r}_c)$, au^{-3}	$\nabla^2\rho(\mathbf{r}_c)$, au^{-5}	λ_1, au^{-5}	λ_2, au^{-5}	λ_3, au^{-5}	ϵ	n
DIC		1.543	0.226	−0.526	−0.373	−0.341	0.189	0.094	0.88
β-MC(1636)		1.636	0.188	−0.318	−0.304	−0.240	0.226	0.267	0.64
β-MC(1712)		1.712	0.161	−0.167	−0.254	−0.160	0.248	0.588	0.51
DIM(1770)		1.770	0.144	−0.008	−0.221	−0.044	0.258	3.99	0.44
α-MC(1783)	C_1–C_6	1.783							
DIM(1826)		1.826							
α-MC(1850)		1.850							
MET		2.235							
DIF		2.269							
DIC		1.568	0.209	−0.419	−0.337	−0.286	0.204	0.178	0.76
β-MC(1636)		1.533	0.227	−0.533	−0.377	−0.339	0.183	0.112	0.88
β-MC(1712)		1.527	0.230	−0.554	−0.383	−0.349	0.177	0.097	0.91
DIM(1770)		1.509	0.238	−0.593	−0.394	−0.367	0.168	0.074	0.97
α-MC(1783)	C_1–C_{11}	1.511	0.238	−0.594	−0.396	−0.365	0.168	0.085	0.97
DIM(1826)		1.507	0.240	−0.602	−0.397	−0.371	0.167	0.070	0.99
α-MC(1850)		1.509	0.239	−0.604	−0.399	−0.370	0.165	0.078	0.98
MET		1.485	0.258	−0.701	−0.434	−0.413	0.147	0.051	1.15
DIF		1.470	0.266	−0.719	−0.459	−0.427	0.166	0.075	1.23
DIC		1.474	0.261	−0.707	−0.437	−0.399	0.129	0.095	1.18
β-MC(1636)		1.472	0.262	−0.715	−0.442	−0.398	0.125	0.110	1.18
β-MC(1712)		1.456	0.268	−0.741	−0.454	−0.403	0.116	0.127	1.25
DIM(1770)		1.457	0.268	−0.742	−0.457	−0.400	0.114	0.143	1.25
α-MC(1783)	C_1–C_2	1.453	0.269	−0.741	−0.456	−0.399	0.115	0.143	1.26
DIM(1826)		1.453	0.269	−0.745	−0.459	−0.398	0.112	0.153	1.26
α-MC(1850)		1.440	0.274	−0.753	−0.463	−0.398	0.108	0.163	1.31
MET		1.405	0.289	−0.803	−0.496	−0.393	0.086	0.262	1.47
DIF		1.409	0.285	−0.781	−0.484	−0.387	0.090	0.251	1.43
DIC		1.344	0.314	−0.854	−0.549	−0.341	0.037	0.610	1.83
β-MC(1636)		1.343	0.314	−0.850	−0.548	−0.339	0.037	0.617	1.83
β-MC(1712)		1.333	0.319	−0.874	−0.558	−0.346	0.030	0.613	1.90
DIM(1770)		1.335	0.318	−0.869	−0.556	−0.344	0.031	0.616	1.89
α-MC(1783)	C_2–C_3	1.340	0.316	−0.860	−0.551	−0.344	0.035	0.602	1.85
DIM(1826)		1.348	0.312	−0.842	−0.543	−0.339	0.040	0.602	1.79
α-MC(1850)		1.351	0.310	−0.842	−0.540	−0.344	0.043	0.570	1.77
MET		1.377	0.299	−0.813	−0.516	−0.357	0.060	0.445	1.61
DIF		1.365	0.303	−0.831	−0.524	−0.361	0.053	0.452	1.67
DIC		1.449	0.270	−0.760	−0.458	−0.405	0.103	0.131	1.27
β-MC(1636)		1.442	0.273	−0.771	−0.464	−0.406	0.099	0.143	1.30
β-MC(1712)		1.427	0.280	−0.625	−0.479	−0.416	0.090	0.151	1.38
DIM(1770)		1.417	0.284	−0.819	−0.487	−0.416	0.085	0.171	1.42
α-MC(1783)	C_3–C_4	1.433	0.277	−0.784	−0.472	−0.406	0.094	0.162	1.34
DIM(1826)		1.431	0.277	−0.783	−0.474	−0.402	0.093	0.179	1.35
α-MC(1850)		1.423	0.281	−0.800	−0.481	−0.407	0.087	0.182	1.39
MET		1.417	0.282	−0.778	−0.481	−0.379	0.083	0.269	1.40
DIF		1.411	0.285	−0.795	−0.487	−0.388	0.080	0.255	1.43
β-MC(1636)		1.471	0.263	−0.721	−0.449	−0.400	0.123	0.113	1.19
β-MC(1712)	C_1–C_{10}	1.456	0.268	−0.745	−0.455	−0.405	0.115	0.123	1.25
α-MC(1783)		1.451	0.270	−0.748	−0.459	−0.402	0.112	0.142	1.27
α-MC(1850)		1.442	0.273	−0.759	−0.465	−0.402	0.107	0.157	1.30
β-MC(1636)		1.347	0.313	−0.844	−0.545	−0.338	0.039	0.612	1.81
β-MC(1712)	C_9–C_{10}	1.336	0.318	−0.866	−0.555	−0.343	0.031	0.618	1.88
α-MC(1783)		1.342	0.315	−0.856	−0.549	−0.343	0.036	0.600	1.84
α-MC(1850)		1.348	0.312	−0.845	−0.543	−0.342	0.040	0.588	1.79
β-MC(1636)		1.445	0.272	−0.764	−0.463	−0.403	0.101	0.149	1.28
β-MC(1712)	C_8–C_9	1.434	0.276	−0.783	−0.471	−0.408	0.096	0.154	1.33
α-MC(1783)		1.432	0.277	−0.786	−0.473	−0.406	0.093	0.165	1.35
α-MC(1850)		1.427	0.279	−0.790	−0.476	−0.404	0.091	0.178	1.36
DIC			0.163	0.199	−0.249	0.203	0.244		
β-MC(1636)			0.160	0.196	−0.244	0.199	0.240		
β-MC(1712)	3MR		0.151	0.167	−0.230	0.151	0.247		
DIM(1770)			0.143	−0.086	−0.219	0.044	0.260		
DIC			0.0208	0.132	−0.018	0.074	0.076		
β-MC(1636)			0.0197	0.122	−0.017	0.068	0.071		
β-MC(1712)	6MR[c]		0.0196	0.122	−0.016	0.065	0.073		
DIM(1770)			0.0188	0.115	−0.016	0.060	0.070		
α-MC(1783)			0.0184	0.113	−0.015	0.061	0.066		
DIM(1826)			0.0176	0.106	−0.014	0.056	0.065		
α-MC(1850)	7MR[c]		0.0177	0.107	−0.014	0.057	0.064		
MET			0.0141	0.084	−0.006	0.037	0.052		
DIF			0.0137	0.081	−0.007	0.040	0.049		

Table III (Continued)

system	critical point	R_c, Å	$\rho(\mathbf{r}_c)$, au^{-3}	$\nabla^2\rho(\mathbf{r}_c)$, au^{-5}	λ_1, au^{-5}	λ_2, au^{-5}	λ_3, au^{-5}	ϵ	n
β-MC(1636)			0.0196	0.122	−0.016	0.067	0.071		
β-MC(1712)	6MR[d]		0.0193	0.120	−0.016	0.064	0.072		
α-MC(1783)			0.0184	0.112	−0.015	0.061	0.067		
α-MC(1850)	7MR[d]		0.0176	0.106	−0.014	0.056	0.064		

[a] See eq 1 for atom numbering. For MC systems, R = CH_3 and R′ = CN. [b] STO-3G calculations with experimental geometries.[1-6] [c] Ring below the CN group in MC systems. [d] Ring below the CH_3 group.

Table IV. Relative Positions[a,b] of the 6MR and 7MR Critical Points (All Quantities in Angstroms)

system[b]		r_{11}	r_1	r_2	r_3	S	h^c	l^c
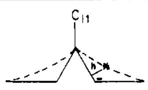	DIC	2.064	1.444	1.434	1.437	0.219	0.007	0.098
	β-MC(1636)	2.035	1.457	1.449	1.453	0.204	0.019 (0.006)	0.129 (0.124)
	β-MC(1712)	1.991	1.458	1.447	1.459	0.188	0.022 (0.013)	0.156 (0.150)
	DIM(1770)	1.974	1.467	1.451	1.472	0.179	0.018	0.177
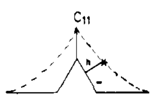	α-MC(1783)	1.938	1.473	1.466	1.470	0.164	0.035 (0.020)	0.176 (0.171)
	DIM(1826)	1.949	1.477	1.473	1.487	0.164	0.022	0.184
	α-MC(1850)	1.902	1.473	1.477	1.485	0.148	0.047 (0.030)	0.190 (0.188)
	MET	1.539	1.554	1.581	1.530	0.020	0.314	0.242
	DIF	1.532	1.552	1.591	1.519	0.028	0.199	0.306

[a] r_i's are the distances between the carbon atoms C_i and the ring critical point, and S is their standard deviations: $S = [\sum_{i=1}^{m}(r_i - \bar{r})^2/m]^{1/2}$, where m is the number of carbon atoms in the ring and $\bar{r}$ is the mean value of the distances r_i. For the MC systems the distances r_i are the average of their values in the two 6/7MR's. [b] Full lines are the projections of CC bonds onto the σ_v plane normal to the C_1–C_6 line. Dotted lines indicate the intersection of the ring charge density surface with the σ_v plane. The star and the h and l values denote the position of the ring critical point. [c] For MC systems the values in parentheses refer to the ring below the CH_3 group.

Table V. Standard Deviations[a] of the CC Distances (S_R) and of the Values of the Charge Density at the Related Bond Critical Point (S_ρ)

system	$10S_R$,[b] Å	$10S_\rho$,[b] au^{-3}
DIC	0.787 (0.803)	0.359 (0.366)
β-MC(1636)	0.690 (0.852)	0.305 (0.374)
β-MC(1712)	0.692 (1.017)	0.310 (0.435)
DIM(1770)	0.647 (1.124)	0.286 (0.460)
α-MC(1783)	0.619	0.274
DIM(1826)	0.580	0.255
α-MC(1850)	0.560	0.248
MET	0.363	0.139
DIF	0.353	0.127

[a] $S_R = [\sum_{i=1}^{m}(R_i - \bar{R})^2/m]^{1/2}$ and $S_\rho = [\sum_{i=1}^{m}(\rho_i - \rho)^2/m]^{1/2}$, where m is the number of bonds considered, R_i and ρ_i are the length of the ith bond and the charge at the related bond critical point, and $\bar{R}$ and $\bar{\rho}$ are the mean values of R_i and ρ_i, respectively. [b] Values in parentheses have been calculated with the inclusion of the C_1–C_6 bond values.

S_ρ, of the charge density ρ at the CC bond critical point. This finding is not surprising, as it has been shown[15] that the $\rho(\mathbf{r}_b)$ values depend linearly on the bond distances. The ratio S_ρ/S_R decreases from 0.46 au^{-3} Å^{-1} in DIC to 0.36 au^{-3} Å^{-1} in DIF and reflects the lowering in strain on going from the dinorcaradienic to the annulenic structure. The last value compares closely with the value (0.35 au^{-3} Å^{-1}) reported for ethane, benzene, ethylene, and acetylene (see the Appendix section). The trend in the S_ρ/S_R ratio indicates also that small CC bond length variations are provided for strained systems at the expense of more significant changes in the charge distribution along the bond paths. The inclusion of the C_1–C_6 bond (when present) in the evaluation of S_ρ and S_R results in a sudden peak in proximity of the bifurcation catastrophe point (see the Appendix section), because of the exceptional C_1–C_6 bond length.

Finally, it is worthwhile to look at the trend in the bond path curvatures, which are fairly represented by the distance d between the bond critical point and the internuclear axis. As shown in Table VI, the C_1–C_{11} bond curvature decreases monotonically from DIC to DIF, because of the opening of the cyclopropyl ring. Correspondingly, the C_2–C_3 and C_3–C_4 bond critical points move inward the 6/7MR, due to the increase of the C_1–C_2–C_3 and C_2–C_3–C_4 bond angles. The ring curvatures in MC reflect the asymmetry of the substitution at C_{11}, as the values for the rings below the methyl and cyano groups closely agree with those of DIM and DIC, respectively.

In the following sections we discuss the individual systems in more detail. As a general consideration, we note that the symmetry constraints force the major axis of the C_1–C_6 bond (when present) to lie[12] in the 3MR and, at the same time, to be properly oriented to overlap with the π clouds of the 6MR's. This fact sketches the possibilities of conjugative coupling of the 3MR to the two butadienyl fragments linked to it. When the C_1–C_6 bond length is close to the value of normal CC bonds, the π-like charge distribution of the 3MR is preserved and the whole cyclopropyl ring behaves as a conjugate π bond. However, *as the C_1–C_6 bond lengthens, the conjugative interaction involves more and more the C_1–C_6 bond alone, as indicated by the drastic increase of its ellipticity*. This mechanism, at its extreme consequences, leads to the annulenic structure. The progressive variation of the 3MR conjugative interaction with the dinorcaradienic skeleton, as dictated by the nature of the C_1–C_6 bond, is nicely illustrated by the sequence of the investigated systems.

Table VI. Bond Critical Point Distances, d, from the Corresponding Internuclear Axis (au)[a]

system	$d_{1,11}$	$d_{1,2}$	$d_{2,3}$	$d_{3,4}$	$d_{1,6}$	$d_{1,10}$	$d_{9,10}$	$d_{8,9}$
DIC	0.150	0.009	−0.015	0.008	0.154			
β-MC(1636)	0.161	0.011	−0.017	0.008	0.136	−0.012	−0.015	0.008
β-MC(1712)	0.154	0.010	−0.020	0.010	0.092	−0.011	−0.018	0.009
DIM(1770)	0.148	−0.011	−0.021	0.010	−0.062			
α-MC(1783)	0.145	0.009	−0.024	−0.001		−0.010	−0.022	−0.010
DIM(1826)	0.138	−0.011	−0.023	−0.010				
α-MC(1850)	0.133	−0.008	−0.028	−0.013		−0.009	−0.025	−0.011
MET	0.044	0.011	−0.041	−0.022				
DIF	0.047	0.010	−0.044	−0.023				

[a] Positive d values mean that the bond path is curved outward from the ring; negative d values indicate that the bond path is curved inward.

Table VII. CC Bond and Ring Critical Point Data for Norcaradiene[a]

numbering	critical point	R_e, Å	$\rho(r_c)$, au^{-3}	$\nabla^2\rho(r_c)$, au^{-5}	λ_1, au^{-5}	λ_2, au^{-5}	λ_3, au^{-5}	ϵ	n	d, au
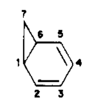	C_1-C_6	1.523	0.232	−0.553	−0.389	−0.339	0.174	0.147	0.92	0.169
	C_1-C_7	1.508	0.238	−0.592	−0.399	−0.357	0.164	0.118	0.97	0.178
	C_1-C_2	1.499	0.252	−0.678	−0.427	−0.388	0.137	0.101	1.09	−0.007
	C_2-C_3	1.324	0.324	−0.885	−0.566	−0.338	0.191	0.675	1.98	−0.004
	C_3-C_4	1.480	0.258	−0.702	−0.437	−0.387	0.122	0.129	1.15	0.015
	3MR		0.179	0.200	−0.273	0.228	0.244			
	6MR		0.021	0.130	−0.017	0.072	0.075			

[a] STO-3G fully optimized geometry.

Dicyano Derivative (DIC). A profitable analysis of DIC molecular structure may be performed by comparison with the related systems 1,1-dicyanocyclopropane (Table II) and norcaradiene (Table VII). The C_1–C_{11} and C_1–C_6 bonds in DIC are longer than the C_1–C_2 and C_2–C_3 bonds in 1,1-dicyanocyclopropane; this fact results in an 8% decrease of the electron density both at the C_1–C_{11} and C_1–C_6 bond critical points and at the ring critical point. In this respect, the 3MR subsystem can be considered as an *electron deficient* 1,1-dicyanocyclopropane. The exceptionally low values of bond orders ($n_{C_1-C_{11}} = 0.76$, $n_{C_1-C_6} = 0.88$) support this picture. However, the polarization induced on the 3MR by the two butadienyl fragments linked to it is evidenced by the CC bond ellipticities, which have increased by 62% and 7% for the C_1–C_6 and the C_1–C_{11} bonds, respectively. The higher increment of the C_1–C_6 bond ellipticity can be explained in terms of the *priviliged conjugative interaction with the butadienyl fragments*, as pointed out by the different values of the overlaps of their major axes with that of the C_1–C_2 bond ($P_{C_{11}-C_1,C_1-C_2} = 0.66$ vs. $P_{C_6-C_1,C_1-C_2} = 0.96$). This finding is strengthened by noting that the bond-to-ring critical point distance in DIC is greater than in 1,1-dicyanocyclopropane. So the usual explanation for the ellipticity increase of the extending bond (C_1–C_6), as due to the migration of the 3MR critical point toward the bond critical point,[12,14] cannot be invoked in this case. By keeping in mind all the considerations above, we may conclude that the peculiar charge distribution of 1,1-dicyanocyclopropane with respect to that of cyclopropane *opposes* and *prevents* the aromatization of the DIC system, though the slight variations observed from 1,1-dicyanocyclopropane to DIC go in this direction.

By comparison of the DIC charge distribution with that of norcaradiene, it appears that, in spite of the relevant differences in the 3MR's, the butadiene-like subsystems behave similarly in both the compounds. Nonetheless, significant differences may be underlined. While the conjugative interaction of the cyclopropyl ring with the butadiene-like subsystem produces only minor changes in the values of $\rho(\mathbf{r}_b)$, n, and ϵ from 1,3-butadiene[12] to norcaradiene (namely, a decrease for the C_2–C_3-type bonds and an increase for the other bonds), such variations are appreciably enhanced in DIC (Tables III and VII), due to a more favorable geometrical arrangement.

In fact, the C_2–C_3 bond order is 1.82 in DIC, an intermediate value between benzene (1.52)[12] and the double bond in propene (2.06).[12] The degree of alignment of the π-electron distribution is also improved: the overlaps of the major axes, beginning with the pair C_1–C_6 and C_1–C_2, are 0.96, 0.97, 1.00 in DIC vs. 0.93, 0.95, 1.00 in norcaradiene. Finally, the sum of the 6MR bond orders is slightly lower in DIC (8.15) than in norcaradiene (8.22), as a straightforward consequence of the electron-withdrawing effect of the cyano groups.

Dimethyl Derivative (DIM). In contrast to DIC, whose dinorcaradienic character is qualitatively explained by the peculiar charge distribution of 1,1-dicyanocyclopropane, no such an indication is offered for DIM by the related 1,1-dimethylcyclopropane. Charge distributions of 1,1-dimethylcyclopropane and cyclopropane are too similar to explain for, at least qualitatively, the relevant geometrical differences between DIM and the parent 1,6-methane[10]annulene.

A tentative explanation of the preferred geometry of DIM may be given on the basis of steric effects, as the bulky CH_3 groups push away the 6MR's and even more the associated density charge surfaces (cf. h values in Table IV).

The unusual existence of two different molecules in the triclinic asymmetric unit cell of DIM can be rationalized only if the packing energy differences can balance the electronic energy gap between the two molecules. A rough estimate of the magnitude of the packing effect[33] indicates that the C_1–C_6 bond is so weak that even a little change in energy, like the packing energy, can be effective in stretching the bond to different lengths.

Topological analysis of the charge distribution in DIM(1770) shows that the C_1–C_6 bond is not only *weak*, as indicated by the $\rho(\mathbf{r}_b)$, $\nabla^2\rho(\mathbf{r}_b)$, and n values, but it is also *labile*,[14] as evidenced by its exceptionally high ϵ value. In fact, since ρ is quite flat along the major axis of curvature ($\lambda_2 = -0.044$) and the bond and ring critical points are close to coalescence (the distance between the bond and the ring critical points is 0.098 Å, to be compared with 0.535 Å in 1,1-dimethylcyclopropane), a singularity in ρ is forming and a structure evolution is at hand. Therefore, it is not surprising that the C_1–C_6 bond has disappeared in DIM(1826).[34] The shift of the bifurcation point to lower values of the CC distance with respect to the ring opening of cyclopropane (1.88 Å)[12] can be ascribed to the incipient aromatization. Since our calculations do not refer to optimized geometries, the indication that the C_1–C_6 bond is present in DIM(1770) and disappears in DIM(1826) cannot be conclusive. However, our topological results, by confirming that the C_1–C_6 bond, if any, is weak and labile, suggest that the two molecules lie on the opposite sides of the potential energy curve for the valence tautomerism (eq 1). In spite of the

(33) An estimate of the order of magnitude of the packing effects was obtained by a molecular mechanics calculation of the packing energy in the real crystal as well as in hypothetical crystals where the two molecules have exchanged their sites or only one type of molecule is present. Differences in packing energy lie in the range 0.2–0.5 kcal/mol.[4]

(34) Since the Hessian matrix of ρ employed in the standard Newton–Raphson procedure to locate critical points[22] was nearly singular in proximity of the C_1–C_6 midpoint, a procedure, based on the steepest descent method, was adopted to check the disappearance of the bond critical point in DIM(1826) and α-MC(1783). ρ decreases monotonically along a line that starts from C_{11}, bisects C_1–C_6, and goes to infinity. The minimum value of $\nabla\rho$ along this line was found in proximity of the C_1–C_6 midpoint and amounts to 9.92 × 10^{-6} and 1.38 × 10^{-2} au^{-4} for α-MC(1783) and DIM(1826), respectively. These values must be compared with the standard threshold of 10^{-13} au^{-4} which is assumed by the AIMPAC program[22] to localize a critical point. The bifurcative nature of the critical point may be inferred from the singularity of the Hessian matrix near the C_1–C_6 midpoint: in α-MC(1783) and in DIM(1826) the character of the Hessian switches from (3,−1) to (3,1), while ρ remains practically constant (for example, in α-MC(1783) the variation of ρ past 0.5 au along the line that bisects C_1–C_6 is less than 5 × 10^{-4} au^{-3}). In spite of similar topological features (i.e., the absence of the C_1–C_6 and 3MR critical points), the charge density distribution in the C_1–C_6–C_{11} plane of DIM(1826) and α-MC(1783) is quite different from that of 1,6-methane[10]annulene. In the last molecule, the charge density value at the C_1–C_6 midpoint has nearly halved, and the character of the Hessian along the above mentioned line is always (3,1). A final check was done to make sure that the singularity in ρ does not bifurcate for further increase of the C_1–C_6 distance, to yield a cage structure (i.e., a (3,3) critical point) and the related three ring structures. Such a behavior was actually found for the [1.1.1]propellane molecule, C_5H_6, when the distance between the bridgehead carbon atoms is increased by more than 0.4 au from its equilibrium value.[13] It can be accounted for by a function (named the unfolding of the elliptic umbilic)[13] of a set of control parameters which define the possible structural changes of the system. In the case of the substituted 1,6-methane[10]annulenes, the lack of formation of a cage structure indicates that the values of the control parameters, dictated by the experimental geometries, do not generate configurations inside that particular structural region. This is not surprising, because of the obvious difference between the 10MR and the two 7MR's, as well as for the too low value of the angle between the planes C_1–C_6–C_{11} and C_1–C_2–C_5.

relevant topological differences, the charge distribution is quite similar in the two DIM's, providing a further indication of the weak interaction provided by the C_1–C_6 bond.

With respect to 1,1-dimethylcyclopropane, the C_1–C_{11} bond ellipticity has a very low value, in agreement with both the release of strain ($\angle C_1$–C_{11}–C_6 is 71.8° in DIM(1770) and 74.6° in DIM(1826)) and the quite different shape of the charge distribution on the 3MR. The charge density at the 3MR critical point of DIM(1770) is about 80% that of 1,1-dimethylcyclopropane. Furthermore, the peculiar position of the ring critical point allows the major axis of the C_1–C_{11} bond to have a high overlap with that of the C_1–C_2 bond ($P_{C_{11}\text{-}C_1,C_1\text{-}C_2}$ is 0.84 and 0.85 for DIM(1770) and DIM(1826), respectively, to be compared with 0.66 for DIC). The latter mechanism (which will be more effective in MET), together with the high value of the C_1–C_2 and C_3–C_4 bond orders, is a clear evidence of the incipient aromatization of the system.

Methylcyano Derivative (MC). Two phases have been found experimentally for MC in the solid state. The crystal structure of the α phase at room temperature is triclinic with two independent molecules in the unit cell, α-MC(1783) and α-MC(1850).[5] At low temperatures α-MC is likely to be metastable.[35] The crystal structure of the β phase is monoclinic.[6] Since the structural parameters of β-MC were found to depend markedly on temperature, both the experimental geometries at room temperature of β-MC(1636) and at −100 °C β-MC(1712) were considered in our calculations.

As in the case of DIC, the partial dinorcaradienic character of MC may be well rationalized by comparison with the related 1-methyl-1-cyanocyclopropane. The clearest indication of this behavior is provided by the low ellipticity of the C_2–C_3 bond (ϵ = 0.09) and the high ellipticity of the C_1–C_2 bond (ϵ = 0.13) in 1-methyl-1-cyanocyclopropane. Since these ellipticity values are intermediate between those of 1,1-dicyanocyclopropane and 1,1-dimethylcyclopropane, it is not surprising that the dinorcaradienic character has the same trend in the β-MC's, as promptly indicated by the value of the C_1–C_6 distance.

There are still some relevant questions which arise from the X-ray analysis of MC. In particular, (i) how is the potential energy profile along the C_1–C_6 bond-length reaction coordinate, in the range of the experimental geometries,[6] (ii) what is the strength of the C_1–C_6 bond in β-MC at low and room temperature,[6,7] and (iii) why do the density deformation maps[6,7] relative to the cyclopropyl ring in β-MC present only a slim evidence of the three positive residues outside the ring,[36] which are expected in bond-strained 3MR's?

The topological analysis of the charge density distribution corresponding to the four experimental geometries of MC may suggest reliable answers to all the above questions. Room temperature X-ray data analysis complies with the existence of three different geometries, due to the influence of three different crystal fields on the free molecular potential. However X-rays cannot discriminate whether the free molecular potential has two minima, corresponding to the dinorcaradienic and the annulenic tautomers separated by a very small energy barrier and with a very low isomerization enthalpy, or it has only one, asymmetric and flat minimum, corresponding to the dinorcaradienic tautomer. The disappearance of the C_1–C_6 bond critical point in α-MC(1783) and α-MC(1850), while indicating the existence of a bifurcation catastrophe point, *strongly suggests the presence of a maximum in the free molecular potential, $E(\mathbf{x})$, in the range of experimental geometries*, along the reaction coordinate of the valence tautomerism (eq 1). In fact, Tal et al.[37] have shown that in general there is a *well-defined correspondence* between structural and energetic instabilities (energetically unstable geometries are saddle points in $E(\mathbf{x})$, i.e., geometries which are at a maximum with respect to one or more of the system's internal motions). A qualitative understanding of this correspondence was provided[37] in terms of a detailed analysis of the nuclear and electronic contributions to the Hellmann–Feynman force exerted on the nuclei, in the neighborhood of the transition state. The electronic contribution can be expressed as an integral over the gradient vector field of the charge density, $\nabla\rho(\mathbf{r},\mathbf{x})$, weighted by the nuclear-electron potentials. Therefore, the sign change of the gradient vector field, $-\nabla_x E(\mathbf{x})$, along the reaction path (demanded by the vanishing of the Hellmann–Feynman force at the transition state) must be ascribed[37] mainly to the drastic *local change* of the gradient field $\nabla\rho(\mathbf{r},\mathbf{x})$ that occurs at the catastrophe point.[38] So the C_1–C_6 bond path (see Figure 1), as long as it exists, pushes C_1 and C_6 atoms closer (dinorcaradienic side of the reaction path) and then turns in a gradient path that, by pulling down the C_{11} atom, increases the C_1–C_6 separation (annulenic side of the reaction path).

With regard to the strength of the C_1–C_6 bond in β-MC(1636) and β-MC(1712), dynamic and static deformation densities, deduced by the X-ray data analysis,[7] agree with the existence of a weak C_1–C_6 bond in β-MC(1636) (as pointed out by a deformation density peak along the C_1–C_6 bond); however, they cannot distinguish between a very weak bonding or nonbonding interaction at room temperature (due to the absence of significant residual electron density between C_1 and C_6). Also deformation electrostatic potentials agree perfectly with these findings.[7] A quantitative answer to this problem is provided by the very low values of $\nabla^2\rho(\mathbf{r}_b)$ for the C_1–C_6 bond: in β-MC(1636) and β-MC(1712) they are just one-half and one-fourth of the ethane value. As can be inferred from Table III, in β-MC(1712) the positive curvature is nearly as high as the most negative curvature (λ_1) and *much higher* of the negative curvature (λ_2) relative to the gradient path connecting the bond and ring critical points. These facts indicate a really weak bond in β-MC(1636) and the lack of any significant bond in β-MC(1712).

The slim evidence of positive residues in the cyclopropyl plane displayed by the experimental deformation density maps can be in part rationalized by the low values of the C_1–C_{11} and C_1–C_6 bond orders in β-MC(1636) and by the less pronounced bond path curvatures, due to the partial release of strain in the 3MR. The values of n, $\rho(\mathbf{r}_b)$, $\nabla^2\rho(\mathbf{r}_b)$, and d reported in Tables III and VI support this hypothesis (also cf. $d_{C_1\text{-}C_2}$ = 0.182 au and $d_{C_2\text{-}C_3}$ = 0.179 au of 1-methyl-1-cyanocyclopropane).

We now turn our attention to some other interesting features. As found in the case of 1-methyl-1-cyanocyclopropane, the asymmetric disubstitution at C_{11} in MC only slightly polarizes the 3MR in a direction perpendicular to it.[39] On the other hand, the 6/7MR's are strongly differentiated with respect to the position of the ring critical points and to the bond path curvatures. Once again the repulsive steric effect of the bulky CH_3 group is evident: in all the MC structures the ring critical point below the CN group is nearly twice as distant from the C_1–C_6–C_2–C_5 plane as the ring critical point below the CH_3 group.

A comparison with the norcaradiene topological results (Table VII) may give an insight of the degree of dienic character of the MC's. A clear-cut progressive departure from the dienic behavior is indicated by the values of the CC bond orders (particularly $n_{C_3\text{-}C_4}$ and $n_{C_8\text{-}C_9}$). It appears that β-MC(1636) is already far from the norcaradiene structure. We also note that the ring below the CH_3 group is nearly always more "aromatic" than that below the CN group (compare, for example, the values of the C_2–C_3 and C_9–C_{10} bond orders).

1,6-Methane[10]annulene (MET). The aromatic character of this compound is well settled on the grounds of both spectroscopic[40]

(35) For this reason, it has been pointed out in ref 6 that the best comparison between DIM and MC is made with the β phase of the latter molecule.

(36) Hartman, A.; Hirshfeld, F. L. *Acta Crystallogr.* **1966**, *20*, 80.

(37) Tal, T.; Bader, R. F. W.; Nguyen-Dang, T. T.; Ojha, M.; Anderson, S. G. *J. Chem. Phys.* **1981**, *74*, 5162.

(38) Tal et al.[37] studied, in particular, the isomerization reaction path from R–CN to R–NC (R = H, CH_3). In this case the catastrophe point is of the conflict type. The drastic local change of the $-\nabla\rho(\mathbf{r},\mathbf{x})$ field in the neighborhood of the transition state is caused by the sudden switching of the R–X bond path from carbon (X = C) to nitrogen (X = N). As long as R is bonded to carbon, the bond gradient path tries to oppose the isomerization to R–NC. In the language of the transition-state theory, the system is climbing a potential barrier, whose maximum occurs at the switching of the bond path to nitrogen.

(39) In β-MC(1636) the 3MR critical point is less than 0.05 au far from the ring surface.

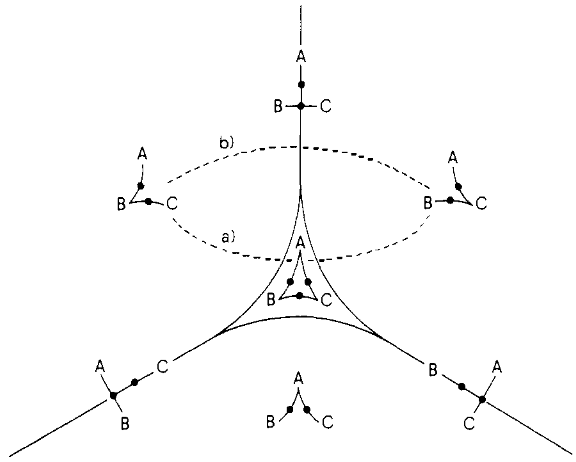

Figure 2. Diagram of all possible structures (indicated by a representative molecular graph) and all mechanisms of structural change ((a) for bifurcation (b) for conflict) for an ABC system.[13]

and X-ray crystal structure determinations.[1] The *degree* of aromaticity of MET may be appreciated by the topological analysis of its charge density function. The CC bond orders and ellipticity values, along the [10]annulenic perimeter, while showing a substantial similarity and a clear-cut π character for the C_1–C_2 (n = 1.47, ϵ = 0.26) and C_3–C_4 (n = 1.40, ϵ = 0.27) bonds, indicate that the C_2–C_3 bond (n = 1.61, ϵ = 0.44) shows a strong similarity with the benzene CC bond (n = 1.58, ϵ = 0.34).

The delocalization of charge along the annulenic perimeter, though quite different from the "dinorcaradienic" framework of DIC, is far from being complete, as evidenced by the differences in CC bond ellipticities and by the uncomplete alignment of the major axes around the 10MR ($P_{C_1-C_2,C_2-C_3}$ = 0.94, $P_{C_2-C_1,C_1-C_{10}}$ = 0.88).

Particular attention should be devoted to the nature of the bridging bonds, C_1–C_{11} and C_6–C_{11}. Their very low ellipticity indicates that the peculiar π character of the 3MR charge distribution has been completely lost: the curvature λ_2, still related to an eigenvector lying in the cyclopropane surface, has actually a very high value, quite close to that of λ_1. Table III shows a progressive strengthening of the bridging bonds on going from β-MC(1636) to MET. Indeed, unlike the compounds previously discussed, the bridging bonds in MET are much stronger (n = 1.15, ϵ = 0.05, $\nabla^2\rho(\mathbf{r}_b)$ = −0.701 au^{-5}) than the CC bond in cyclopropane and resemble the central bond of *trans*-1,3-butadiene (n = 1.11, ϵ = 0.10, $\nabla^2\rho(\mathbf{r}_b)$ = −0.697 au^{-5}),[12] except for the low value of their ellipticity, which is more similar to that of the CC single bond in propene (ϵ = 0.03).[12] These facts, together with the very high overlap of the major axes of the C_1–C_{11} (C_6–C_{11}) and C_1–C_2 bonds ($p_{C_{11}-C_1,C_1-C_2}$ = 0.93 to be compared, for example, with the corresponding value of 0.84 in α-MC(1850)), indicate the existence of two really strong σ bonds, with a partial π character, which may enter in conjugation with the [10]annulenic framework. Though C_{11} participation to the aromatic skeleton involves, in terms of resonance theory, only ionic structures, its importance is pointed out not only by the peculiar properties of the bridging bonds but first of all by the previously described elevation of the 7MR critical point (h = 0.31 Å, Table IV). The relative orientation of the two planes tangent to the charge density surface at the two 7MR critical points is given by the corresponding λ_1 eigenvectors. In MET their overlap is 0.73, which corresponds to an angle of 42.8°, while in DIC the two planes are at 25.8° (P_{λ_1,λ_1} = 0.90). These considerations sketch the *existence*, in a resonant way, of two 6π-electron conjugated systems, instead of the more fundamental 10π-electron system, and provide a tentative explanation of the far better stability of MET with respect to the extremely reactive π-isoelectronic unbridged [10]annulenes.[41] In fact the [10]annulenes show both spectroscopic[42] and theoretical[4,3] evidence of very alternating CC bond lengths (typically around 1.50 and 1.33 Å in all the investigated isomers) and consequently bear few if any signs of aromaticity, in spite of the $4n + 2$ Hückel rule fulfillment.

Difluoro Derivative (DIF). As noted above, the STO-3G minimal basis set is not capable to reproduce the essential features of the related 1,1-difluorocyclopropane. Because of this fact, we prefer not to analyze the DIF results in detail (see Table III), even if they correlate rather well with those of the remaining systems.

However, it is noteworthy that the 3-21G results for the 1,1-difluorocyclopropane (Table II) provide an excellent prediction of DIF behavior. In fact the C_2–C_3 bond has a very low value of $\rho(\mathbf{r}_b)$ and a very high value of ellipticity with respect to the C_1–C_2 bond or the CC bond of cyclopropane. Moreover, the C_2–C_3 bond critical point and the ring critical point are close to each other (0.79 vs. 1.12 au for the C_1–C_2 bond-to-ring critical point distance).

Such topological results, which are opposite to that of 1,1-dicyanocyclopropane, clearly help the C_1–C_6 bond breaking.

Finally, the comparison of 1,1-difluorocyclopropane with the remaining 1,1-disubstituted cyclopropanes (Table II) justifies the position of DIF along the reaction path of the valence tautomerism (eq 1) in a quite straightforward manner.

Acknowledgment. We are grateful to Prof. R. F. W. Bader for the generous gift of a copy of the AIMPAC package of programs.

Appendix

The Bader topological theory of molecular structure has been discussed extensively in literature (see, for example, ref 13). Here we summarize only the essential points which are pertinent to the discussion of our results.

The molecular charge distribution is described by the scalar function $\rho(\mathbf{r},\mathbf{x})$, where $\mathbf{r}$ is a vector of the ordinary three-dimensional space R^3 and $\mathbf{x}$ represents any set of nuclear coordinates in the space of nuclear configurations R^q. The chemical structure of a molecule can be unambigously assigned by determining the number and kind of *critical points* in its electronic charge distribution, points where the gradient of ρ (the vector $\nabla\rho$ of the three first derivatives of ρ) vanishes. The collection of the nine second derivatives of ρ, evaluated at the position of the critical point $\mathbf{r}_c$, defines a real symmetric matrix (Hessian). The principal curvatures of ρ at $\mathbf{r}_c$ (i.e., the three eigenvalues of the Hessian, λ_i) define the *rank p* and the *signature q* of the critical point (p,q). The rank of a critical point is given by the number of non-zero eigenvalues, and its signature is the algebraic sum of their signs. There are only four possible nondegenerate critical points in R^3, namely (3,−3), (3,−1), (3,1), and (3,3). The critical points of the type (3,3) and (3,−3) are associated with a local minimum and a local maximum in $\rho(\mathbf{r})$, respectively. With minor exceptions, due to inadequacies of basis sets, a local maximum in $\rho(\mathbf{r})$ can occur only at the position of a nucleus.

The collection of all the integral curves (named *gradient paths*) $\mathbf{r}(s) = \mathbf{r}_0 + \int_0^s \nabla\rho[\mathbf{r}(t),\mathbf{x}]dt$, which are solutions of the differential equation A1 for some initial value $\mathbf{r}(0) \equiv \mathbf{r}_0$, and which in general will terminate at a given nucleus, defines a subset in R^3, which is the *basin* of that nucleus. Therefore, the nucleus acts as an

$$d\mathbf{r}(s)/ds = \nabla\rho[\mathbf{r}(s),\mathbf{x}] \qquad \text{(A1)}$$

attractor for its basin. The union of an attractor and its basin defines an *atom* in the molecule. Since a nucleus is the only three-dimensional attractor in R^3, the space of the molecular charge distribution is partitioned into disjoint regions, each containing only one nucleus (see Figure 1). Two adjacent basins are separated by an interatomic surface, $S(\mathbf{r})$, through which the

(40) Vogel, E.; Roth, H. D. *Angew. Chem., Int. Ed. Engl.* **1964**, *3*, 228.

(41) (a) Burkoth, T. L.; Van Tamelen, E. E. In "Nonbenzenoid Aromatics"; Snyder, J. P., Ed.; Academic Press: New York, 1969, Chapter 3. (b) Van Tamelen, E. E. *Acc. Chem. Res.* **1972**, *5*, 186. (c) Masamune, S.; Darby, N. *Ibid.* **1972**, *5*, 272.

(42) Masamune, S.; Hojo, K.; Hojo, K.; Bigam, G.; Rabenstein, D. L. *J. Am. Chem. Soc.* **1971**, *93*, 4966.

(43) Farnell, L.; Kao, J.; Radom, L.; Schaefer, H. F., III. *J. Am. Chem. Soc.* **1981**, *103*, 2147.

gradient vector field of ρ has zero flux (i.e. $\nabla\rho(\mathbf{r})\cdot n(\mathbf{r}) = 0$, $\forall \mathbf{r} \in S(\mathrm{r})$, where $n(\mathbf{r})$ is the unit vector normal to the surface at $\mathbf{r}$). Due to its zero-flux properties, any interatomic surface is generated by the gradient paths which terminate at a critical point contained in the same surface. This is a (3,−1) critical point, i.e., a two-dimensional attractor, and is called a *bond critical point*, $\mathbf{r}_b$. In fact, the eigenvector of the positive curvature at $\mathbf{r}_b$ gives the initial direction of two gradient paths which terminate at two neighboring nuclei, thus defining a *bond path*. Along a bond path ρ is a maximum with respect to any lateral displacement. The network of bond paths for a molecule in a given nuclear configuration defines the *molecular graph*. All the neighbor nuclear configurations which have *equivalent* molecular graphs belong to the same *structural region* or *phase*. To each structural region is associated a single stable *molecular structure*, i.e., a unique set of molecular graphs which contain the same number of bond paths, linking the same nuclei.

A point in the nuclear configuration space R^q, whose molecular graph indicates a discontinuous structural change as a consequence of a continuous change of the nuclear coordinates, the parameters which control the behavior of the system, is called a *catastrophe point* and is associated to an unstable molecular structure. Catastrophe points are of two different types. A *bifurcation* catastrophe point corresponds to breaking or making of bonds; it indicates a *singularity* in the charge distribution ρ, i.e., a degenerate critical point.

At a *conflict* catastrophe point two initially unequal attractors come into balance in their competition for a bond path. In Figure 2 a two-dimensional cross section of the structure diagram for an ABC system is reported, indicating the two possible reaction mechanisms (the bifurcation and the conflict reaction) for changing the structure A–B–C into the structure B–C–A.

Also the critical points of the type (3,1) and (3,3) have a chemical meaning. The eigenvectors associated with the two positive eigenvalues of the Hessian matrix evaluated at a (3,1) critical point generate a surface (named *ring surface*) in which the (3,1) critical point (*ring critical point*) is a minimum in ρ. The axis perpendicular to the ring surface at the ring critical point, along which $\rho(\mathbf{r}_c)$ is a maximum, is the intersection of the boundaries of the atomic basins forming the ring (see Figure 1A,B).

The eigenvectors associated with the three positive eigenvalues of a (3,3) critical point, a local minimum in ρ, generate an infinity of gradient paths which originate at the critical point and bound a closed region of space, i.e., a *cage*. A (3,3) critical point, a *cage critical point*, is common to all the interatomic surfaces of the atoms forming the cage.

So far we have introduced some definitions and concepts which are related to the topology of a molecular structure and its structural evolution. Now we turn our attention to the quantitative analysis of the characteristics of a bond as they can be inferred by the properties of ρ at the bond critical point.

$\rho(\mathbf{r}_b)$, the value of ρ at the bond critical point $\mathbf{r}_b$, is correlatd with the equilibrium internuclear distance R_e. For the CC bond $\rho(\mathbf{r}_b)$ increases as R_e decreases, and this trend is well described by the linear relationship[15]

$$\rho(\mathbf{r}_b) = aR_e + b \qquad \text{(A2)}$$

where a and b depend on the basis set ($a = -0.348$ au^{-3} Å^{-1}, $b = 0.777$ au^{-3} for STO-3G). The linear relationship (A2) was obtained by fitting $\rho(\mathbf{r}_b)$ vs. R_e for ethane, benzene, ethylene, and acetylene and is well satisfied for all CC bonds having R_e equal to the *bond path length* R_b. CC bonds with curved bond paths obey (A2) provided that the bond path lengths rather than R_e are considered. The curvature of a bond path may be appreciated by the d value of the distance between the bond critical point and the internuclear axis, as well as by the ratio R_b/R_e. A positive d values indicates that one is dealing with a strained system. In fact this behavior has been observed in those cases where the models of directed valence[44] predict the existence of strained bonds (in cyclopropane $d = 0.182$ au and $R_b/R_e = 1.018$ at the STO-3G level). A negative d value is found when the bond paths are curved toward the interior of a ring, in order to maximize the stability of a system. This is the case, for example, of the bridging hydrogen network in diborane. The $\rho(\mathbf{r}_b)$ values can be also correlated with the bond order n through the relationship[12]

$$n = \exp\{A[\rho(\mathbf{r}_b) - B]\} \qquad \text{(A3)}$$

where A and B depend on the basis set ($A = 1.23$ Å^3, $B = 1.63$ Å^{-3} for STO-3G). Since $\rho(\mathbf{r}_b)$ values are linearly related to R_b rather than R_e, eq A3 is not a usual bond order–bond length relationship but is directly related to the distribution of electronic charge that results at the electrostatic equilibrium. This allows one to group together bonds with similar chemical characteristics, in spite of differences in their R_e values.

Very useful information on the shape of the charge distribution along the bond is given by the principal curvatures (λ_i) of ρ at $\mathbf{r}_b$ and the associated principal axes of curvature, i.e., the three eigenvalues and the corresponding eigenvectors of the Hessian of ρ at $\mathbf{r}_b$. The asymmetry of the charge distribution in a plane perpendicular to the bond path may be appreciated by the ratio $\epsilon = \lambda_1/\lambda_2 - 1$ of the two negative curvatures of ρ at the bond critical point (the eigenvalues are ordered in increasing value). The ϵ quantity, called *ellipticity* of the bond, gives a measure of the deviation of the charge distribution from cylindrical symmetry and thus can be correlated with the amount of π character of a bond. For the CC bond in ethane, λ_1 and λ_2 are obviously degenerate and ϵ is zero. If ϵ is greater than zero, the eigenvectors associated with λ_1 and λ_2 define a unique pair of axes perpendicular to the bond path: the charge density decreases faster along the *minor axis* of curvature (λ_1) and decreases slower along the *major axis* of curvature (λ_2). In conjugated systems (e.g., *trans*-1,3-butadiene) the major axes of the CC bonds are all parallel[12] and point in a direction coincident with that of the maximum in π distribution of the usual orbital theory. The same behavior is found in systems presenting hyperconjugative interactions (e.g., propene). The *overlap* of the major axes of neighboring bonds (the overlap is determined by taking the scalar product of the eigenvectors defining the major axes of the two bond critical points) gives the extent of charge delocalization in noncoplanar conjugated systems.[14] We use the symbol $P_{i\text{-}j,j\text{-}k}$ to indicate the overlap of the major axes of the neighboring bonds i–j and j–k. So the values of P and ϵ are an obvious measure of the degree of π delocalization in a molecule:[14] in benzene all P values of the carbon framework are 1.00 and the corresponding ϵ values are equal. Conjugative and hyperconjugative effects may also be qualitatively characterized by the $\rho(\mathbf{r}_b)$, n, and ϵ values of the bonds involved.[12,14] The *trace* of the Hessian, i.e., the sum of its eigenvalues, at the bond critical point, $\nabla^2\rho(\mathbf{r}_b)$, provides a further cumulative indication of the nature of a bond.[15] For a covalent bond, the pile-up of charge in the bonding region results in a low positive curvature (λ_3) of ρ along the bond path and in large negative curvatures (λ_1 and λ_2) in the perpendicular directions. Therefore, the value of $\nabla^2\rho(\mathbf{r}_b)$ is less than zero and becomes more and more negative as the bond order increases, since the charge distribution along the bond path is increasingly flat.

Registry No. Cyclopropane, 75-19-4; 1,1-dicyanocyclopropane, 1559-03-1; 1,1-dimethylcyclopropane, 1630-94-0; 1-cyano-1-methylcyclopropane, 78104-88-8; 1,1-difluorocyclopropane, 558-29-2.

(44) Coulson, C. A.; Moffit, W. E. *Phil. Mag.* **1949**, *40*, 1.